Synopsis of thesis entitled

Catalytic materials based on Transition metals & Phosphomolybdate : Designing & Application in some organic transformations

To be submitted to

The Maharaja Sayajirao university of Baroda

For the Degree of

DOCTOR OF PHILOSOPHY

IN

CHEMISTRY

BY

Jaykumar Patel

Department of Chemistry,

Faculty of Science,

The Maharaja sayajirao University of Baroda,

Vadodara-390020, Gujarat, India

May, 2022

Introduction

Heteropoly acids (HPAs) are acidic form of Polyoxometalates (POMs), formed by different mononuclear oxoanions. These oxoanions tend to polymerize, by dehydration at low pH forming polyanion and water.They exhibit a wide range of molecular sizes, compositions and architectures [1]. HPAs have the general formula $[X_xM_mO_y]^{q-}$, in which X is the hetero atom, usually a main group element (e.g., P, Si, Ge and As), and M is the addenda atom, being a d-block element in high oxidation state, usually $V^{IV/V}$, Mo^{VI} or W^{VI}. These compounds are always negatively charged although the negative density is widely variable depending on the elemental composition and the molecular structure [1-2].

With the development of HPA chemistry, various types of structures were discovered. Of all the different types of HPAs, the Keggin type HPAs are the most extensively studied because of its ease in synthesis, high thermal as well as chemical stability [3]. The ideal Keggin structure, $[XM_{12}O_{40}]^{3-}$ has T*d* symmetry and consists of a central XO_4 tetrahedron (X = central heteroatom) surrounded by twelve MO_6 octahedra (M = addenda atom). The twelve MO_6 octahedra form four groups of three edge-shared octahedra, the M_3O_{13} triplet, which have a common oxygen vertex connected to the central heteroatom. HPAs have several advantage such as robust oxoanionic nature, Brønsted acidity, reversible redox behaviour, high stability, reducing, encapsulating ability and most importantly, the structural mobility (by two way, i. molecular levels and ii. available exchangeable protons) [4-14].

Designing of POMs can be done at molecular level by four ways: (i) Removal of M=O unit from the keggin unit can lead to the formation of lacunary HPAs (ii) Transition metal can be substituted in the lacuna forming transition metal substituted heteropoly acids (TMSHPAs) (iii) by exchange of available protons of HPAs with Metal salt and (iv) HPAs supported on various supports. All four basic designed strategies shown in scheme 1.

1. **Lacunary Heteropoly acid**

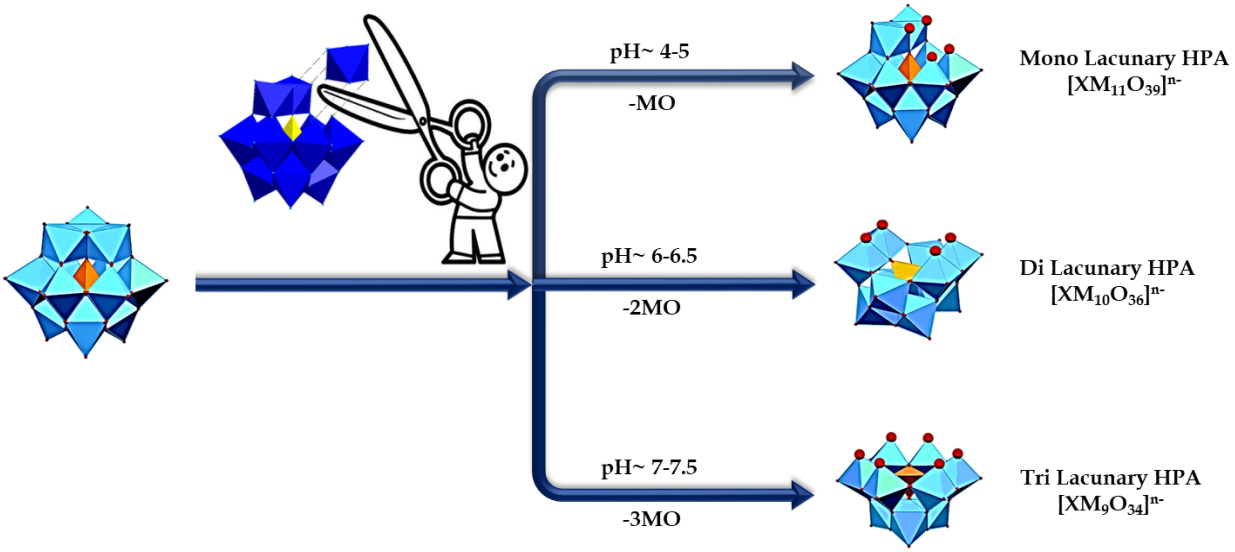

2. **Metal substituted Heteropoly acid**

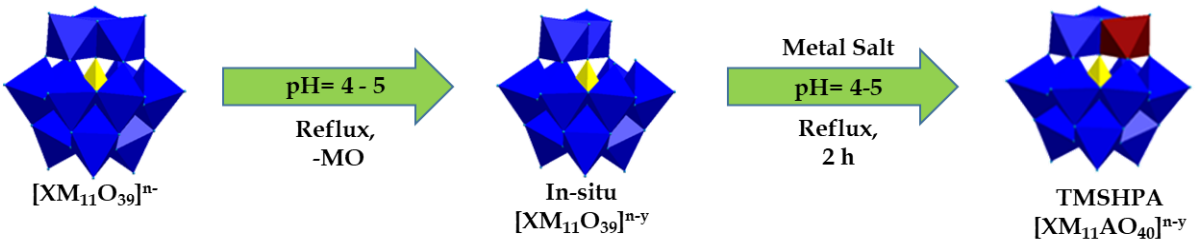

3. **Metal salt of Heteropoly acids by direct method (Homogeneous)**

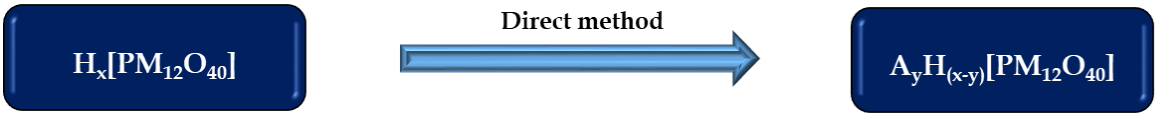

Where A is metal

4. **Supported metal salt of Heteropoly acids by direct method (Heterogeneous)**

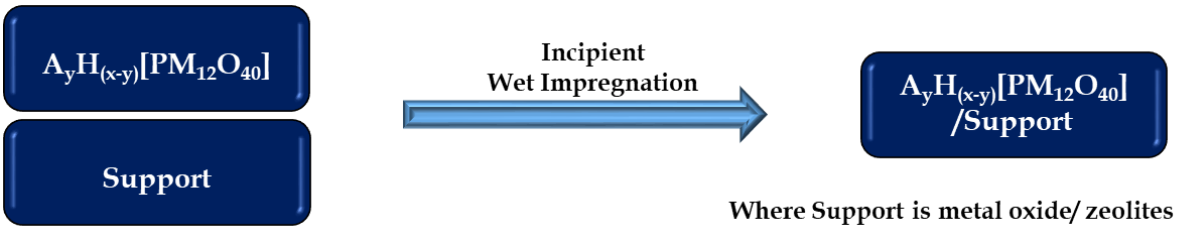

Where Support is metal oxide/ zeolites

5. Metal exchanged Heteropoly acids supported on support by ion exchange method (Heterogeneous)

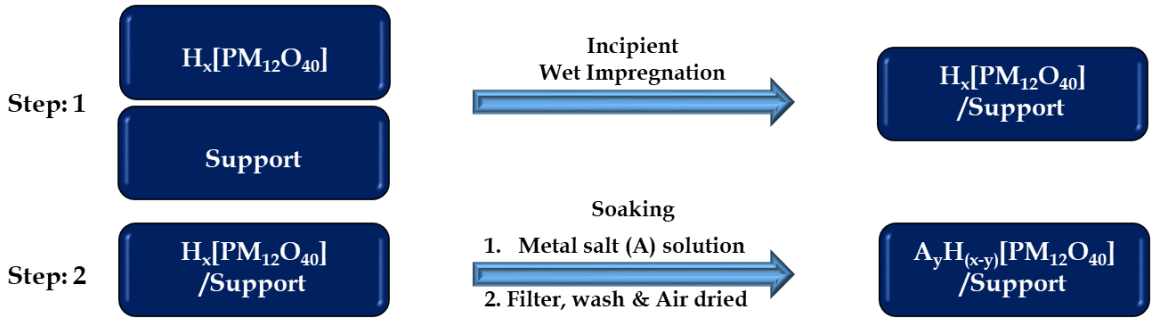

Amongst various hetropoly acdis, phosphomolybdic acid is known for their good redox property. A literature survey shows that there are number of reports on the synthesis, characterization and catalytic activity of phosphotungstic acid and silicotungstic acid. But at the same time, reports on phosphomolybdic acid are comparatively less explored. It was reported that, because of high decomposition and equilibrium rate, the isolation of metal substituted phosphomolybdic acid from aqueous solution is quite difficult. So it was thought of interest to synthesize, isolate and stabilize transition metal substituted or exchanged phosphomolybdic acid.

Considering these advantages and their ability to activate transition metal ions, it was thought of interest to synthesize a series of transition metal substituted or exchanged phosphomolybdic acid. Fe, Pd and Ni were chosen as they are known to be redox active metal ions and they have wide range of catalysis, such as coupling, hydrogenation, oxidation, alkylation, acylation and many more.

Objectives of work

- To tune the structural and redox properties of lacunary phosphomolybdates by insertion of transition metal ions into the lacuna to form transition metal substituted phosphomolybdates (TMSPM).
- To synthesize transition metal (Ni, Fe and Pd) exchanged anchored phosphomolybdates on ZrO_2 as a support.
- To characterize synthesized materials by various techniques such as Elemental analysis, TG-DTA, FT-IR spectroscopy, Raman Spectroscopy, ^{31}P NMR, UV-Vis spectroscopy, XPS, Powder XRD, BET Surface area, SEM, TEM and HRTEM.
- To use the synthesized materials as catalysts for liquid phase oxidation, hydrogenation, C-C coupling, and oxidative esterification.
- To study all the respective reaction parameters such as ratio of substrate to catalyst, temperature, pressure, time and solvent for maximum conversion as well as product selectivity.
- To study reaction mechanism.
- To propose best catalyst for organic transformation.

The work is divided in to the three part based on transition metal

Part A: Designing of catalysts based on Iron & Phosphomolybdic acid

Chapter 1: Cesium salt of iron substituted phosphomolybdic acid ($PMo_{11}Fe$): Synthesis, characterization and hydrogenation reactions

Chapter 2: Iron exchanged phosphomolybdic acid supported on zirconia ($Fe\text{-}PMo_{12}/ZrO_2$): Synthesis, characterization and hydrogenation reactions

Part B: Designing of catalysts based on Palladium & Phosphomolybdic acid

Chapter 1: Cesium salt of palladium substituted phosphomolybdic acid ($PMo_{11}Pd$): Synthesis, characterization and hydrogenation reactions

Chapter 2: Palladium exchanged phosphomolybdic acid supported on zirconia ($Pd\text{-}PMo_{12}/ZrO_2$): Synthesis, characterization and One-pot Suzuki–Miyaura cross coupling/ nitro hydrogenations

Part C: Designing of catalysts based on Nickel & Phosphomolybdic acid

Chapter 1: Nickel exchanged phosphomolybdic acid supported on zirconia ($Ni\text{-}PMo_{12}/ZrO_2$): Synthesis, characterization and hydrogenation reactions

Chapter 2: Nickel salt of phosphomolybdic acid (NiHPMA): Synthesis, characterization and application for oxidative esterifications

Part A: Designing of catalysts based on Iron & Phosphomolybdic acid

Chapter 1: Cesium salt of iron substituted phosphomolybdic acid ($PMo_{11}Fe$): Synthesis, characterization and applications for hydrogenation of styrene

Synthesis:

1.825 g of $H_3PM_{12}O_{40}$ was dissolved in minimum quantity of water and maintained pH 4.3 followed by addition of saturated sodium bicarbonate ($NaHCO_3$). The obtained solution was heated at 80 ^{0}C with stirring. To the resultant solution, 0.404 g (1 mmol) of $Fe(NO_3)_3$ dissolved in

minimum amount of water, was added. The ultimate pH of the resulting mixture was maintained 4.3 by adding $NaHCO_3$ solution then refluxed at 80 ^{0}C for 1 h and filtered hot. Finally, to this saturated CsCl (5 mmol, 0.8418 gm) solution was added and the resulting yellow color precipitates were filtered, washed with water. It was further dried at room temperature and designated as $PMo_{11}Fe$.

Characterization:

Synthesized material was characterized by elemental analysis, EDX, TGA FT-IR, Raman spectroscopy, ^{31}P NMR, ESR, XPS and powder XRD.

EDX mapping confirms the presence of Cs, P, Mo, Fe and O in synthesized materials. The observed EDX values of the elements (Cs:25.88%, P:1.27%, Mo:41.39%, Fe:2.08%, O:28.97%) were in good agreement with the that of calculated values (Cs:25.99%, P:1.21%, Mo:41.28%, Fe:2.18%, O:28.79%).

TGA showed 2.5% weight loss in the range of 30-120 ^{0}C, which is attributed to adsorbed water. Further, 1.3% weight loss is observed from 150 to 350 ^{0}C corresponding to crystalline water. After that, no other significant weight loss is observed which indicate that the synthesized material is stable up to 500 ^{0}C. Based on elemental and thermal analysis, the formula of the complex is proposed as $Cs_5[PMo_{11}O_{39}Fe(H_2O)].5H_2O$

The FT-IR spectrum of PMo_{12} (figure 1a) shows characteristic stretching vibration bands at 1060, 965, 870, 790 cm^{-1} attributed to P-O, M=O, Mo-O_b-Mo and Mo-O_c-Mo stretching respectively. The FT-IR spectra of PMo_{11} shows all characteristic bands of PMo_{12} with splitting in P-O stretching band at 1064 and1045 cm^{-1} which indicates the formation of lacuna. Similarly, the FT-IR spectra of $PMo_{11}Fe$ (figure 1a) shows splitting in P-O band at 1070, and 1054 cm^{-1} due to decrease in symmetry of central atom PO_4 tetrahedron unit by removing MoO unit and other bands at 964 cm^{-1}(M=O), 873 cm^{-1} (Mo-O_b-Mo) and 783 cm^{-1} (Mo-O_c-Mo), shows slight shifting because of the distortion introduced by one Mo replaced with Fe. Also, it shows one additional band at 516 cm^{-1} for Fe-O stretching frequency.

Raman spectra of PMA (figure 1b) show peaks at 1005, 987, 916, 620 and 251 cm^{-1} corresponding v_s Mo=O, v_{as} Mo=O, v_{as} Mo-O_b-Mo, v_{as} Mo-O_c-Mo and v_{as} Mo-O_a stretching vibration respectively. Raman spectra of $PMo_{11}Fe$ show intense peak at 947 cm^{-1} and shoulder at 928 cm^{-1} were due to

the symmetric (v_s) and asymmetric (v_{as}) stretching of Mo=O_t respectively, sharp and broad peak at 904 cm^{-1} and 603 cm^{-1} corresponding to v_{as} Mo-O_b-Mo stretching, and peak at 223 cm^{-1} corresponding to v_{as} Mo-O_c-Mo stretching. Also it shows peak at 367 cm^{-1} corresponding to v_{as} O_a-P-O_a (central tetrahedral PO_4) stretching indicates that Keggin unit remains intact. $PMo_{11}Fe$ shows slight shifting due to insertion of Fe into lacuna, formation by removing one Mo and obtained result is in good agreement with reported ones. ^{31}P MAS NMR of $PMo_{11}Fe$ (figure 1c) was found to be silent due to insertion of Fe in lacuna by formation of paramagnetic spices (P-O-Fe^{3+}).

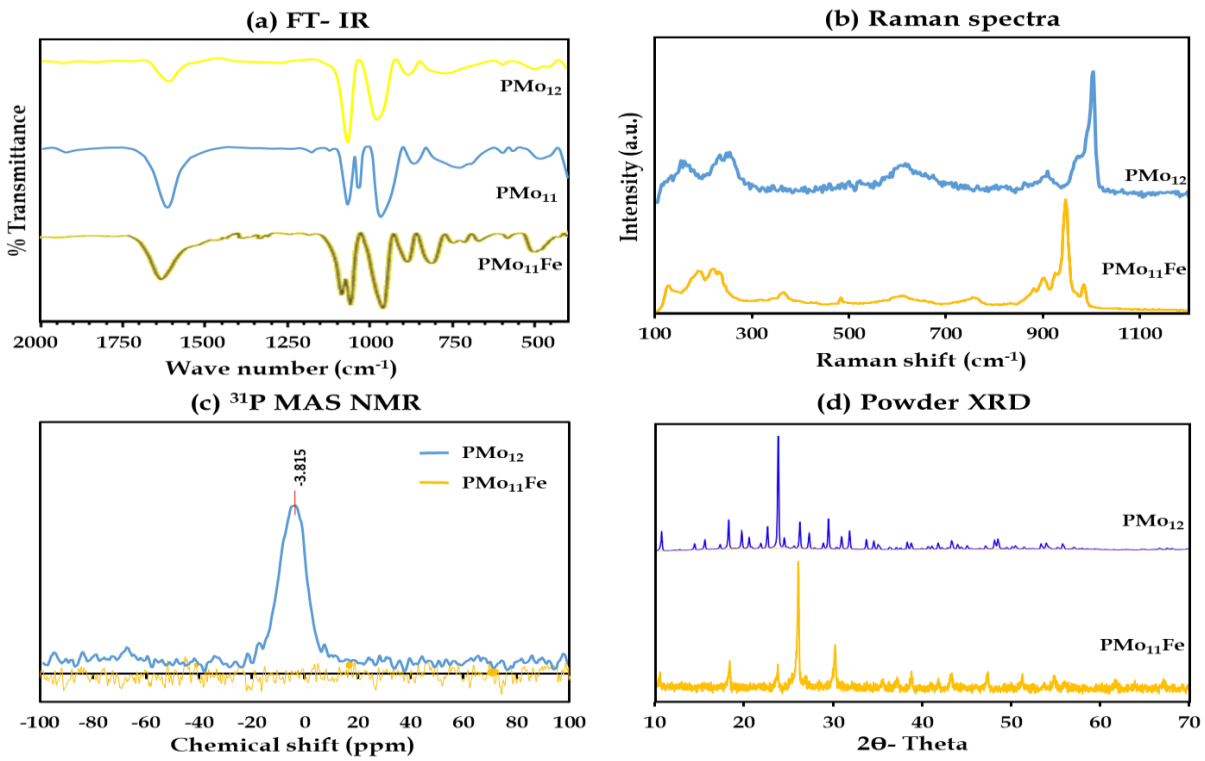

Figure 1. (a) FT-IR spectra, (b) Raman spectra, (c) ^{31}P MAS NMR and (d) powder XRD of fresh catalyst

The XRD patterns of PMo_{12} (figure 1d) show all characteristic peaks in the range of 15^0 to 35^0 of 2Θ. Similarly, XRD pattern of $PMo_{11}Fe$ (figure 1d) show all the characteristic peaks of keggin unit, with slight shift due to Fe incorporation in PMo_{11} and also shows additional sharp peaks at 18.34, 23.88, and 30.28 attributed to the presence of Fe. Above studies shows that keggin unit remains preserved even after Fe in corporation.

The full range (5000–2500 G) X-band liquid nitrogen temperature ESR spectrum for $PMo_{11}Fe$ gives a single hyperfine spectrum with an isotropic signal, observed at g=4.3, which assigned Fe(III) with distorted octahedral geometry and it integrated (incorporated) with phosphomolybdate in high-spine (3+ state).

The XPS of $PMo_{11}Fe$ show two doublets intense peak at binding energy i) 233 and 235 eV, ii) 397 and 416 eV corresponding to 3d5/2, 3d3/2, 3p3/2 and 3p1/2 energy level of Mo^{6+} respectively. Also intense peak at 721 eV corresponds to 2p1/2 energy level of Fe^{3+}. Two additional high intense peaks at binding energy 532 eV and 724 eV is attributed to O1s and $Cs3d_{5/2}$, respectively.

The FT-IR, Raman spectroscopy, powder XRD confirms the insertion of Fe in to lacuna by replacing one MoO unit. The ^{31}P MAS NMR, ESR and XPS analysis confirmed that Fe is present in 3+ state with high spin and paramagnetic in nature.

Catalytic activity

The catalytic efficiency of $PMo_{11}Fe$ was evaluated for styrene hydrogenation. Effect of various reaction parameters such as solvent, substrate-catalyst ratio, reaction time, temperature, and H_2 pressure were studied to obtain maximum conversion.

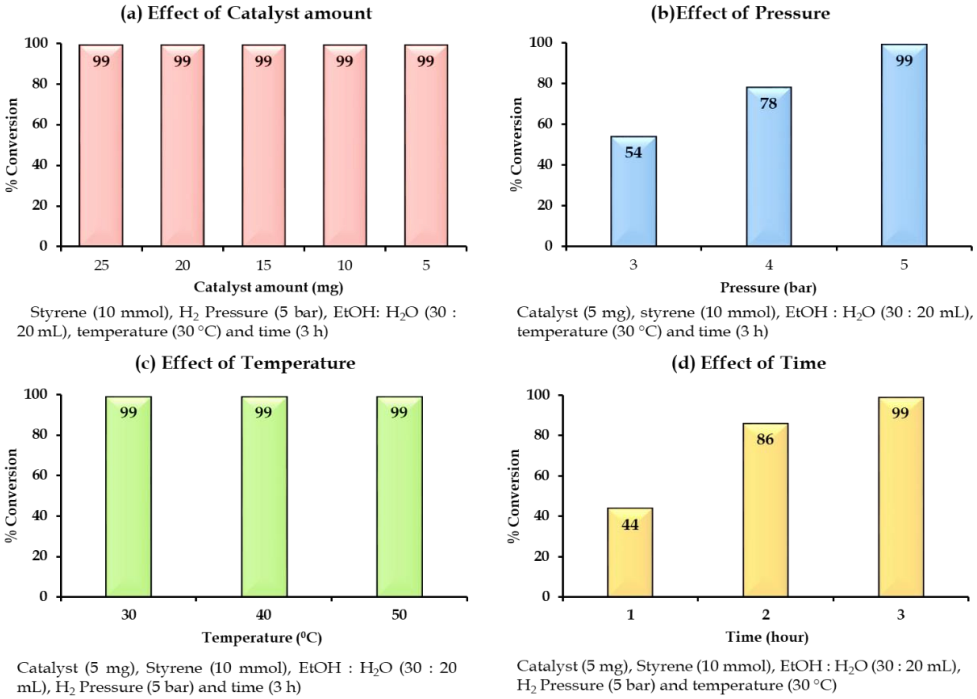

Figure 2. Optimization of reaction parameters

Amount of catalyst was optimized by varying it from 25-5 mg, keeping all other parameters constant for obtaining maximum conversion (figure 2a). Initially, it was observed that 100% conversion was achieved with 25 mg of catalyst. However, with further decrease in the catalyst amount, there is no substantial change in the conversion up to 5 mg of catalyst. Consequently, 5 mg catalyst amount was optimized for achieving maximum 99% conversion. Effect of hydrogen pressure on reaction was screened from 3-5 bar, obtained result shows in the figure 2b. The result obtained shows that with an increase in pressure from 3 bar to 5 bar, the conversion rate also increased. Optimum 99% conversion was achieved at 5 bar H_2 pressure and is considered to be an optimized reaction pressure. The effect of temperature on the reaction was also evaluated from 30-50 °C with an interval of 10 °C and obtained results are shown in figure 2c. No increase in %conversion with temperature was found and hence 30 °C temperature was optimized. Finally effect of reaction time was optimized by keeping all other parameters constant, for optimum conversion. It was seen (figure 2d) that with an increase in time from 1 h to 3 h, increase in the %conversion i.e, 99% conversion was obtained in 3h. Therefore, 3 h was optimized for the reaction.

The effect of differant solvent show that MeOH and EtOH showed high 89% and 99% conversion respectively, may due to their reducing nature as compared to H_2O (70%) and CH_3CN gave only 20% conversion, because of its oxidizing nature. Reactions were also carried out using binary (aqueous medium) solvent systems such as MeOH: H_2O (1:1.5) and EtOH: H_2O (1:1.5), and drop in %conversion as compared to neat solvent was observed. This may be due to the dilution effect which may decrease their reducing nature. Interestingly, CH_3CN: H_2O resulted in rise of conversion from 20 to 54% as addition of water decreased the amount of CH_3CN in system. Also, the dispersion of styrene in MeOH, EtOH, H_2O and CH_3CN is different, which can lead to diffusion problem and then effect the styrene conversion. Based on these results, reaction was optimized using EtOH: H_2O solvent and results are showed in table 3. Amongst all 1.5: 1 ratio of EtOH: H_2O gave optimum 99% conversion.

The optimized conditions for maximum 70% conversion are: substrate /catalyst ratio (5081), catalyst (5 mg), Styrene (10 mmol), EtOH:H_2O (30:20 mL), H_2 pressure (5 bar), time (3 h), temperature (30 ^{0}C), TON (5081).

In order to investigate the role of individual components, control experiments were performed without H_2, without catalyst, using $Fe(NO_3)_3$ with active amount of Fe and with active amount of PMo_{11} under optimized reaction conditions. It was seen from the obtained result that H_2 pressure and catalyst both are essential for the reaction progress. Both $Fe(NO_3)_3$ and PMo_{11} gave low conversion in aqueous medium. This indicates that Fe of $PMo_{11}Fe$ is responsible for the reaction.

In order to check heterogeneity of $PMo_{11}Fe$, hot filtration test was carried out. The obtained result indicates that no leaching of Fe from $PMo_{11}Fe$ was observed during the reactions. This study indicates that the catalyst is truly heterogeneous in nature to be recycled and reused. The check sustainability of catalyst, the catalyst was recycled by simple centrifugation and reused for the next cycle. The obtained result show that there is no significant change in conversion up to two cycle. This indicates that catalyst is stable and can be reused up to several cycles.

Characterization of regenerated catalyst

The regenerated catalyst was characterized by EDX, FT-IR, ESR and XPS analysis for the confirmation of the catalyst structure retention. The regenerated catalyst was designated as R-$PMo_{11}Fe$. For R-$PMo_{11}Fe$, EDX values (Cs: 26.00%, P: 1.21%, Mo: 41.28%, Fe: 2.18%, O: 28.79%) are in good agreement with fresh one, indicating that there was no leaching of Fe during the reaction. EDX mapping (figure 3a) shows the presence of Cs, P, Mo, Fe and O in regenerated catalyst.

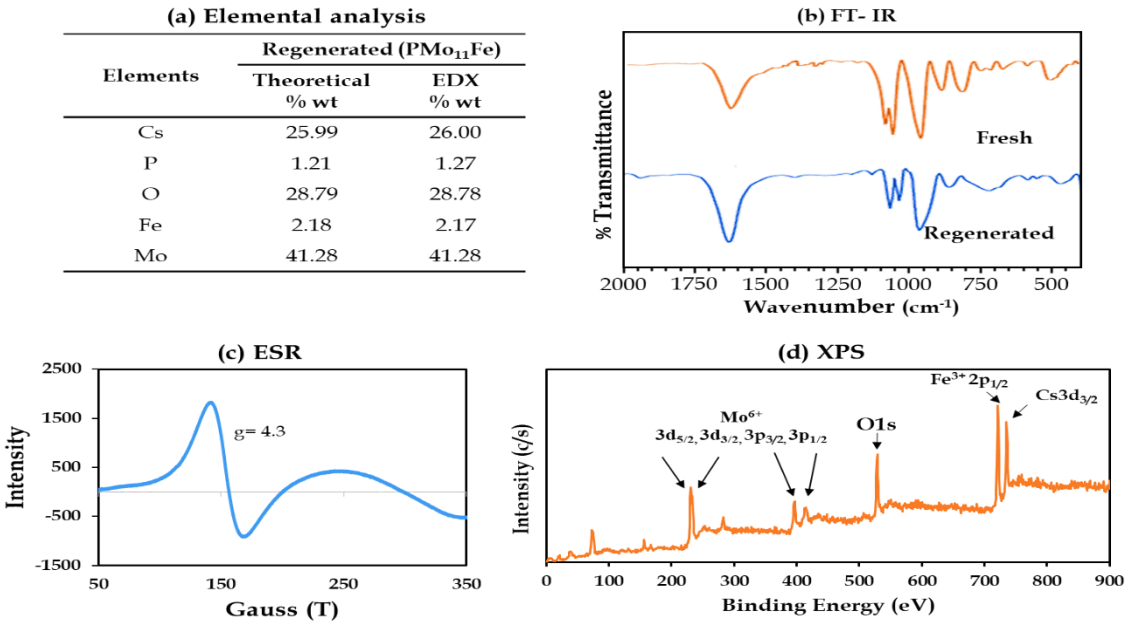

Elements	Regenerated ($PMo_{11}Fe$)	
	Theoretical % wt	EDX % wt
Cs	25.99	26.00
P	1.21	1.27
O	28.79	28.78
Fe	2.18	2.17
Mo	41.28	41.28

Figure 3. (a) EDX mapping, (b) FT-IR, (c) ESR and (d) XPS of regenerated catalyst

The FT-IR spectrum of fresh and regenerated catalysts (figure 3b) show almost identical spectrum without any significant shift in characteristic band of regenerated catalyst (R-$PMo_{11}Fe$) as compared to $PMo_{11}Fe$, indicating that the structure of the catalyst remains unchanged even after regeneration. The ESR spectra of R-$PMo_{11}Fe$ gives a single hyperfine spectrum with an isotropic signal, observed at g=4.3, which is identical with fresh catalyst, $PMo_{11}Fe$. The XPS of R-$PMo_{11}Fe$ is showed intense peaks at 234, 236, 397 and 416 eV which correspond to 3d, and 3p energy level of Mo(VI) and also shows intense peak at 724 eV which corresponds to 2p energy level of Fe(III). The obtained spectrum is identical with fresh one, indicates sustainability of the catalyst.

Chapter 2: Iron exchanged phosphomolybdic acid supported on zirconia (Fe-PMo_{12}/ZrO_2): Synthesis, characterization and applications for hydrogenation of cyclohexene

To design the catalyst, the advantage of available counter protons of phosphomolybdic supported on zirconia exchange iron was exploited. Hydrous Zirconia (ZrO_2) and phosphomolybdic supported on zirconia were synthesized by following the same method reported by us. Iron exchanged supported phosphomolybdic acid was synthesized via exchanging the available protons of PMA. 1 g PMo_{12}/ZrO_2 was soaked with 25 mL 0.05 M $Fe(NO_3)_3$ aqueous solution with stirring for 24 hours. The solution was filtered, washed with distilled water to remove excess iron and dried in air at room temperature. The obtained yellow colored material was designated as Fe-PMo_{12}/ZrO_2.

The synthesized materials were characterized by characterized by elemental analysis (EDX), TGA FT-IR, ^{31}P NMR, ESR, XPS, powder XRD and HDDF-STEM.

The EDX mapping shows the presence of all elements. Found EDX value of Fe (0.54 wt%) and Mo (14.05 wt%) in Fe-PMo_{12}/ZrO_2 are in good agreement with theoretical calculated values of Fe (0.68 wt%) and Mo(14.14 wt%). TGA of Fe-PMo_{12}/ZrO_2 show 9.3% weight loss up to 100 ^{0}C due to the absorbed water. No weight loss observed up to 500 ^{0}C indicating the stability up to 500 ^{0}C.

Fe-PMo_{12}/ZrO_2 (Figure 4a) shows the all the characteristic bands of PMo_{12} at 1075 cm^{-1} (P-O_a), 948 cm^{-1}(M=O_t) and 887 cm^{-1} (Mo-O_b-Mo) as well as ZrO_2 at 1620 cm^{-1} (H-O-H), 1381 cm^{-1} (O-H-O) and a broad band at 700-400 cm^{-1} (Zr-O-H). However, minor shift in all bands may be attributed to the change in counter cation environment of PMo_{12}. Additional band of Fe-O

stretching appears as a shoulder at 509 cm^{-1} due to its superimposition with that of broad band corresponding to Zr-O-H.

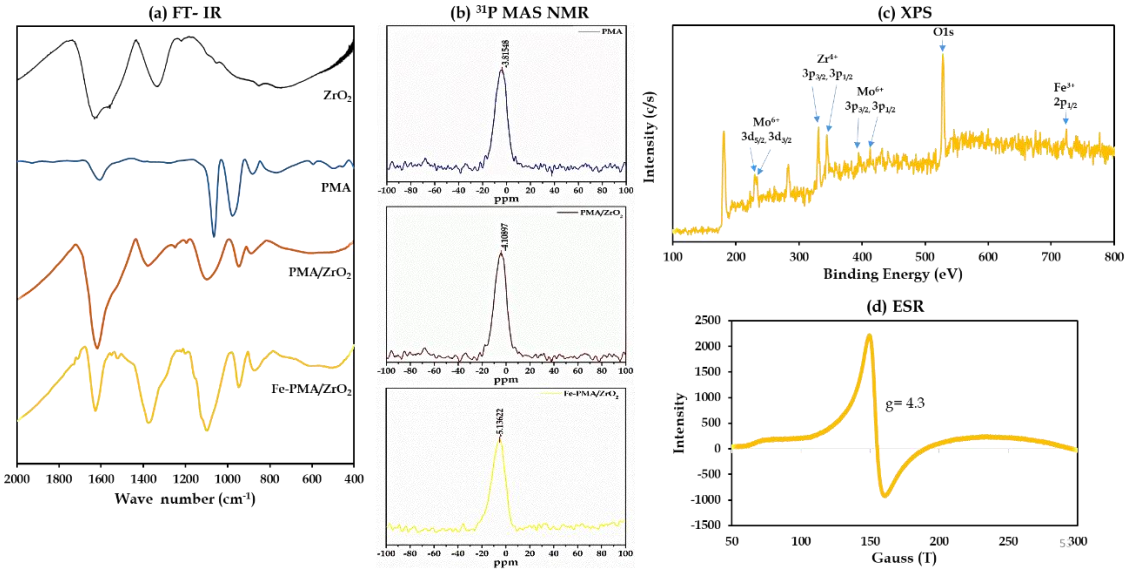

Figure 4. (a) FT-IR spectra, (b) ^{31}P MAS NMR, (c) XPS and (d) ESR spectra of fressh catalyst

^{31}P MAS NMR of Fe-PMo_{12}/ZrO_2 (figure 4b) shows significant up filed shifting in peak from -5.13 ppm compered to PMo_{12}/ZrO_2 (-4.16 ppm). This is due to change in electronic environment of PMo_{12} as Fe gets exchanged with counter proton of PMo_{12}/ZrO_2. The XPS analysis of Fe-PMo_{12}/ZrO_2 was recorded as shown in figure 4c. A binding energy peak at 724 eV corresponding $Fe2p_{1/2}$ energy level, conforming the presence of Fe^{3+}. Similarly, spine-orbit binding energy level for Mo^{6+} was observed as two doublet i) at 233 and 235 eV Corresponding to $3d_{5/2}$ and $3d_{3/2}$ energy level ii) at 397, and 416 eV Corresponding to $3p_{3/2}$ and $3p_{1/2}$ energy level. Two additional intense peaks at binding energy 331 eV and 345 eV attributed to $Zr3p_{3/2}$ and $Zr3p_{1/2}$. Also, highly intense binding energy peak at 532 eV attributed to O1s for oxygen present in PMA as well as ZrO_2. The temperature ESR spectrum of Fe-PMo_{12}/ZrO_2 (figure 4d) shows a single isotropic hyperfine spectrum at g=4.3, which is allocated to Fe present in +3 states.

The BET surface area of ZrO_2 is 170 m^2g^{-1} whereas the surface area of PMA/ZrO_2 is 204 m^2g^{-1}, which is significantly higher as compared to support ZrO_2 because of the strong interaction between PMo_{12} and support. However the surface area of Fe-PMo_{12}/ZrO_2 was found to be 208 m^2g^{-1}, this may be due to the exchange of Fe with available protons of PMo_{12}. The powder XRD pattern of ZrO_2, PMo_{12}, PMo_{12}/ZrO_2 and Fe-PMo_{12}/ZrO_2 were recorded. The XRD pattern

of ZrO_2 show amorphous nature of support. PMo_{12} showed all characteristic peaks in the range of 15^0 to 35^0 of 2Θ. The XRD pattern of PMo_{12}/ZrO_2 does not show any characteristics peak of PMo_{12}, suggesting that PMo_{12} is highly disperse in non-crystalline from on the support (ZrO_2). The XRD pattern of Fe-PMo_{12}/ZrO_2 similar in comparison of PMo_{12}/ZrO_2, indicating the Fe highly depressed on non-crystalline PMo_{12}/ZrO_2. HAADF-STEM images of Fe-PMo_{12}/ZrO_2 also confirm the homogeneous dispersion of Fe over the PMo_{12}/ZrO_2.

The catalytic activity of Fe-PMo_{12}/ZrO_2 was evaluated by performing Hydrogenation of cyclohexene. In order to achieve maximum conversion the effect of different reaction parameters (figure 5) such as catalyst amount, temperature, pressure, time and solvent were studied.

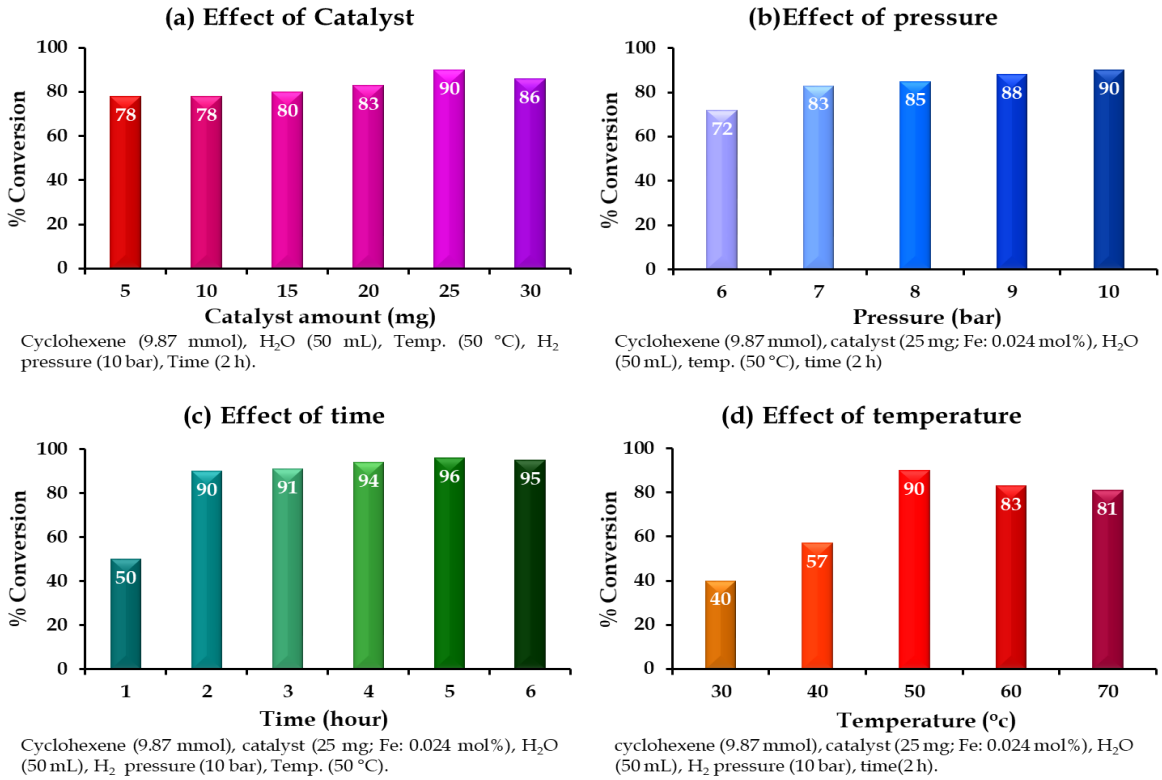

Figure 5. Optimization of reaction parameters

The optimized conditions for the maximum 90% conversion with 3742 TON are: catalyst amount (25 mg; Fe: 0.024 mol%), cyclohexene (9.87 mmol), H_2O (50 mL), H_2 pressure (10 bar), time (2 h) and temp. (50 °C), and Substrate/Catalyst ratio (4157/1).

The control experiment indicates that Fe is the real active species responsible for the reaction. Whereas hot filtration and recyclability test confirms the no leaching of Fe from Fe-PMo_{12}/ZrO_2 as well as it can be reused upto three cycle without significant loss in catalytic activity. In order to check the stability, the regenerated catalyst was characterized by EDX, FT-IR, ESR and XPS analysis which confirms the retention of catalyst structure even after recycled.

Part B: Designing of catalysts based on Palladium & Phosphomolybdic acid

Chapter 1: Cesium salt of palladium substituted phosphomolybdic acid ($PMo_{11}Pd$): Synthesis, characterization and hydrogenation reaction

1.825 g of $H_3PM_{12}O_{40}$ was dissolved in minimum quantity of water and maintained pH 4.7 followed by addition of saturated sodium bicarbonate ($NaHCO_3$). The obtained solution was heated at 80 ^{0}C with stirring. To the resultant solution, 0.1773 g (1 mmol) of $PdCl_2$ dissolved in minimum amount of water, was added. The ultimate pH of the resulting mixture was maintained pH 4.7 by adding $NaHCO_3$ solution then refluxed at 80 ^{0}C for 1 h and filtered hot. Finally, to this saturated CsCl (5 mmol, 0.8418 gm) solution was added, the resulting brown color precipitates were filtered and washed with water, dried at room temperature and designated as $PMo_{11}Pd$(II). Finally the synthesized material was charged in a par reactor under 1 bar H_2 pressure, at 40 ^{o}C for 30 min to reduce Pd(II) to Pd(0). The obtained black colored material was designated as $PMo_{11}Pd$.

The synthesized material were characterized by elemental analysis (EDX), FT-IR, ^{31}P MAS NMR, XPS, powder XRD, TEM, HRTEM and HAADF-STEM.

Elemental analysis shows the presence of all the expected elements and the found values from EDX of the elements (Cs:25.43%, P:1.21%, Mo:40.28%, Pd:4.09%, O:28.97%) were in good agreement with the that of calculated values (Cs:25.60%, P:1.19%, Mo:41.25%, Pd:44.11%, O:28.70%). FT-IR shows the presence of all the characteristic bands of PMo_{11} in the synthesized material $PMo_{11}Pd$, confirming the retention of the Keggin structure. ^{31}P MAS NMR shows significant down filed shifting in peak from 7.797 ppm, confirm that Pd is inserted in to the lacuna with retention of structure. XRD pattern of the $PMo_{11}Pd$ showed all the characteristic peaks of Keggin unit, with slight shift due to Pd incorporation with PMo_{11}. The XPS spectra indicates the presence of PdNPs as well as Mo in VI oxidation states, confirming no reduction of Mo(VI) during

the synthesis of the materials. TEM and HRTEM images clearly shows the presence of PdNPs, whereas HAADF –STEM images confirmed that high dispersion of pd.

The catalytic efficiency of $PMo_{11}Pd$ was evaluated towards levulinic acid hydrogenation. In order to achieve maximum conversion the effect of different reaction parameters such as catalyst amount, Formic acid, temperature, time and solvent was studied.

The effect of catalyst amount and effect of formic acid was optimized. Further, optimization of effect of time, temp., solvent, control experiments, heterogeneity test and characterization of regenerated catalyst are in progress…..

Chapter 2: Palladium exchanged phosphomolybdic acid supported on zirconia(Pd-PMo_{12}/ZrO_2): Synthesis, characterization and One-pot Suzuki–Miyaura cross coupling/ nitro hydrogenation

Palladium was deposited on PMo_{12}/ZrO_2 via exchanging the available protons of PMA. 1 g of PMo_{12}/ZrO_2 was soaked with 25 mL of 0.05 M aqueous solution of $PdCl_2$ for 24 h with stirring. The solution was filtered, washed with distilled water in order to remove the excess of $PdCl_2$ and dried in air at room temperature. The resulting (brown colored) material was designated as Pd(II)- PMo_{12}/ZrO_2. Finally, the synthesized material was charged in a Parr reactor under 1 bar H_2 pressure, at 40 °C for 30 min to reduce Pd(II) to Pd(0). The obtained (black colored) material was designated as Pd- PMo_{12}/ZrO_2.

Synthesized material was characterized by elemental analysis, FT-IR, ^{31}P MAS NMR, XPS, BET surface area, powder XRD, TEM, HRTEM and HAADF-STEM.

The gravimetric analysis shows 0.43 %wt of Pd in Pd(II)-PMo_{12}/ZrO_2 as well as elemental analysis by EDX also shows 0.45 %wt of palladium in Pd-PMo_{12}/ZrO_2. The TGA of the Pd-PMo_{12}/ZrO_2 shows the 9.3 % weight loss up to 200 °C due to the loss of adsorbed water molecules. No weight loss was observed up to 500 °C indicating the stability of the catalyst up to 470 °C. The FT-IR spectrum (figure 6a) of Pd- PMo_{12}/ZrO_2 shows the characteristic bands at 1078, 956, 878 and 790 cm^{-1} corresponding to stretching vibration of P=O, Mo=O and Mo-O-Mo with significant shift, may be due to the change the counter cation environment of PMA by insertion of Pd.. Here, additional band corresponding to Pd-O band is not observed, this may be due to the merging of band with Zr-O.

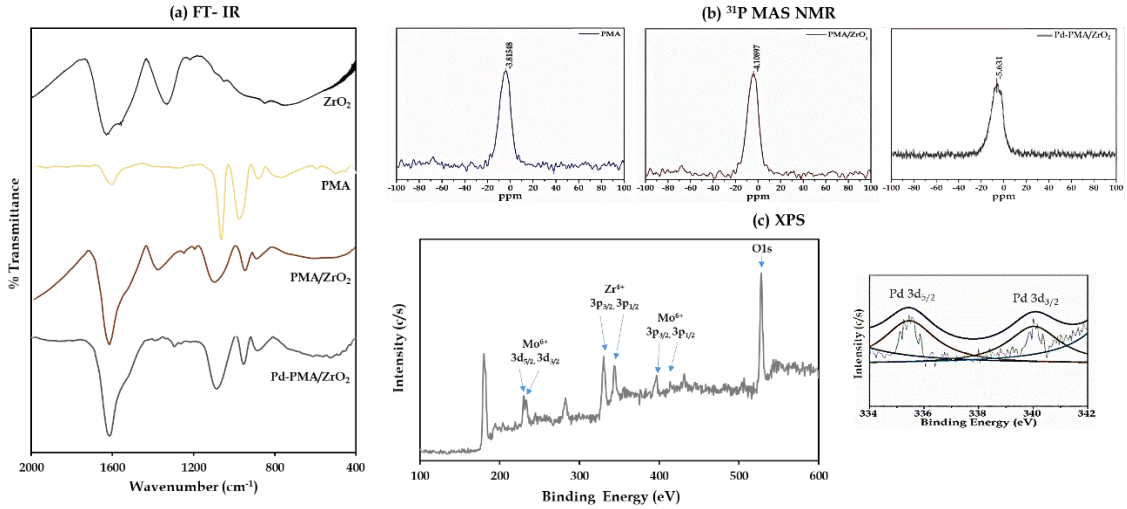

Figure 6. (a) FT-IR, (b) ^{31}P MAS NMR and (c) XPS of fresh catalyst

^{31}P MAS NMR of Pd- PMo_{12}/ZrO_2 (figure 6b) shows significant up filed shifting in peak from -4.1 to -5.61 ppm as compared to PMo_{12}/ZrO_2. This is due to change in electronic environment of PMA as Pd gets exchanged with counter proton of PMo_{12}/ZrO_2.X-ray photoelectron spectroscopy (XPS) of Pd- PMo_{12}/ZrO_2 was recorded (figure 6c). It displayed two low intense peaks at 334.78 eV and 340.16 eV, corresponding to two distinct spin-orbits 3d5/2 and 3d3/2 respectively of the metallic palladium (Pd^0), which confirms the formation of PdNPs. Two different intense peaks at 233 eV and 235 eV corresponding to spin-orbits 3d5/2 and 3d3/2, of Mo^{6+} respectively, confirms that Mo(VI) has not reduced during reduction of Pd(II) to Pd(0).

The small increase in surface area of the Pd(II)-PMo_{12}/ZrO_2 (209 m^2 g^{-1}) as compared to that of PMo_{12}/ZrO_2 (204 m^2 g^{-1}) indicates exchange of Pd with available proton of PMo_{12} over PMo_{12}/ZrO_2. It is very interesting to note that there is a drastic increase in the value of surface area of Pd- PMo_{12}/ZrO_2 (228 m^2 g^{-1}) as compared to that of Pd(II)- PMo_{12}/ZrO_2 (208 m^2 g^{-1}), confirming the reduction of Pd(II) to Pd(0) and is in good agreement with the known fact that nanoparticles have higher surface area than the parent one. The XRD patterns of ZrO_2, PMo_{12}/ZrO_2 and Pd- PMo_{12}/ZrO_2 catalysts were recorded. The XRD patterns of ZrO_2 show the amorphous nature of the support. Whereas, PMo_{12}/ZrO_2 does not show any characteristic diffraction line indicating that a high dispersion of PMo_{12} in non-crystalline form on the surface of ZrO_2. In XRD patterns of Pd-PMo_{12}/ZrO_2, absence of any crystalline peak corresponds to Pd(0), which is due to the low concentration of Pd(0) on the surface of the catalyst as well as high dispersion of PdNPs on the surface of PMo_{12}/ZrO_2.

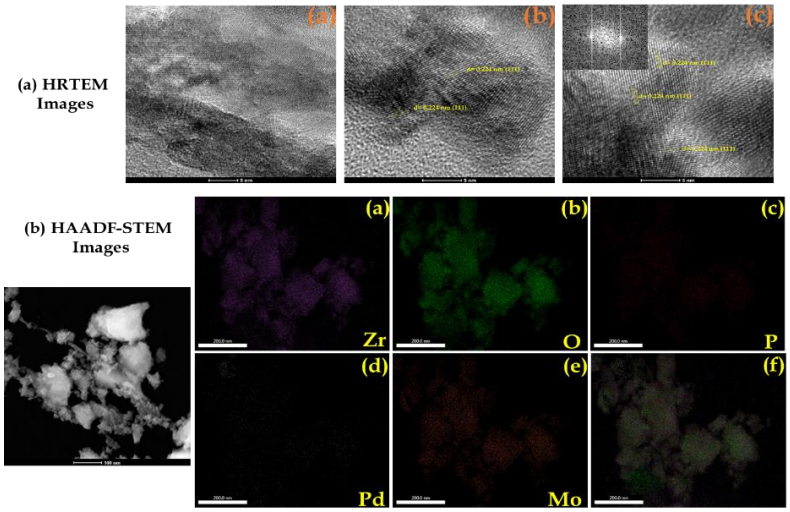

Figure 7. (a) HRTEM images and (b) HAADF-STEM images of fresh catalyst

TEM and HRTEM (figure 7a) images of the fresh catalyst indicate the non-crystalline and uniform dispersion of Pd(0) in the synthesized material. The dark uniform suspension in the amorphous nature of the catalyst (figure 7b) indicates the presence of very tiny Pd(0) nanoparticles (PdNPs) throughout the morphology without any aggregate formation, confirming the stabilization PdNPs by PMo_{12}.

The catalytic activity of the catalyst was evaluated towards One-pot Suzuki–Miyaura cross coupling/ nitro hydrogenation reaction. As we achieved excellent activity of Pd-PMA/ZrO_2 for SM cross-coupling, further Pd-PMo_{12}/ZrO_2 was evaluated for One-pot Suzuki–Miyaura cross coupling/ nitro hydrogenation reaction. To achieve maximum conversion various reaction parameter were optimized such as, catalyst amount, pressure, time and temperature.

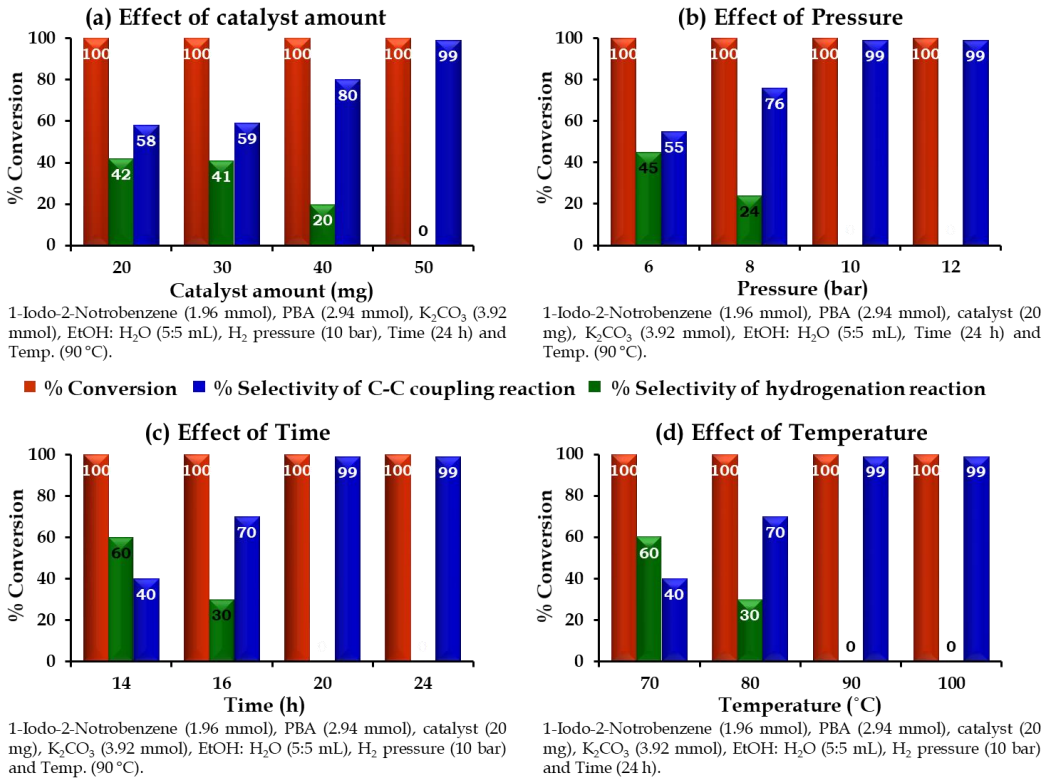

Figure 9. Optimization of reaction parameters

Based on above study, the optimized conditions for 100% conversion with 99% selectivity of 2-aminobiphenyl are: iodobenzene (1.96 mmol), phenylboronic acid (2.94 mmol), catalyst (50mg, active amount of Pd: 0.225 mg), K_2CO_3 (2.96 mmol), C_2H_5OH:H_2O (5:5 mL), pressure (10 bar), time (24 h) & temp. (90 °C) with, TON (918), TOF (38) and substrate ratio/ catalyst (927).

The control experiments were carried out with $PdCl_2$, PMo_{12}, ZrO_2, PMo_{12}/ZrO_2 and Pd-PMo_{12}/ZrO_2 under optimized conditions. It is seen from the obtained results that PMo_{12}, ZrO_2 and PMo_{12}/ZrO_2 are inactive towards the reaction. Almost same conversion was found in the case of $PdCl_2$, and Pd-PMo_{12}/ZrO_2. This indicates that Pd is real active species responsible for the reaction.

The heterogeneity and recyclability tests were carried out for Pd-PMo_{12}/ZrO_2 by centrifuging the catalyst from the reaction mixture. This study also indicates that PMo_{12} plays an important role in binding the palladium very strongly and thus does not allow its leaching of palladium into the reaction mixture, making it, a true heterogeneous catalyst to recycle and reuse up to three cycles without any appreciable change in activity. In order to check the stability, the regenerated catalyst

was characterized by EDX, FT-IR and XPS analysis which confirms the retention of catalyst structure and XRD indicates the presence of highly dispersed PdNPs over the surface of the catalyst, even after recycling.

Part C: Designing of catalysts based on Nickel & Phosphomolybdic acid

Chapter 1: Nickel exchanged phosphomolybdic acid supported on zirconia (Ni-PMo_{12}/ZrO_2): Synthesis, characterization and hydrogenation reaction

Nickel was deposited on PMo_{12}/ZrO_2 via exchanging with the available protons of PMo_{12}. 1 g of PMo_{12}/ZrO_2 was soaked with 25 mL of 0.04 M aqueous solution of $Ni(CH_3CO_2)_2$ for 24 h with stirring. The solution was filtered, washed with distilled water in order to remove the excess of $Ni(CH_3CO_2)_2$ and dried in air at room temperature. The resulting green colored material was designated as Ni(II)-PMo_{12}/ZrO_2.

Synthesized material was characterized by elemental analysis, FT-IR, ^{31}P MAS NMR, XPS, BET surface area and Powder XRD.

The synthesized material was characterized by various physico-chemical techniques in which, gravimetric as well as EDX showed that the presence of Ni was 0.29 % wt. FT-IR, ^{31}P MAS NMR and powder XRD indicated the retention of the Keggin unit even after PMo_{12} support on ZrO_2 as well as exchange of Ni with available protons of PMo_{12}/ZrO_2. BET of synthesized material shows small increased in surface area (208 m^2 g^{-1}) as compared to PMo_{12}/ZrO_2, which further indicates that Ni is exchanged only with proton of PMo_{12}. N_2 sorption isotherms confirms the retention of the basic structure in the synthesized material. XPS confirmed the presence of Ni(II) and Mo(VI).

The catalytic efficiency of the catalyst was evaluated towards levulinc acid hydrogenation reaction and various reaction parameters (effect of catalyst, formic acid, time, temperature and solvent) were optimized to achieve maximum conversion.

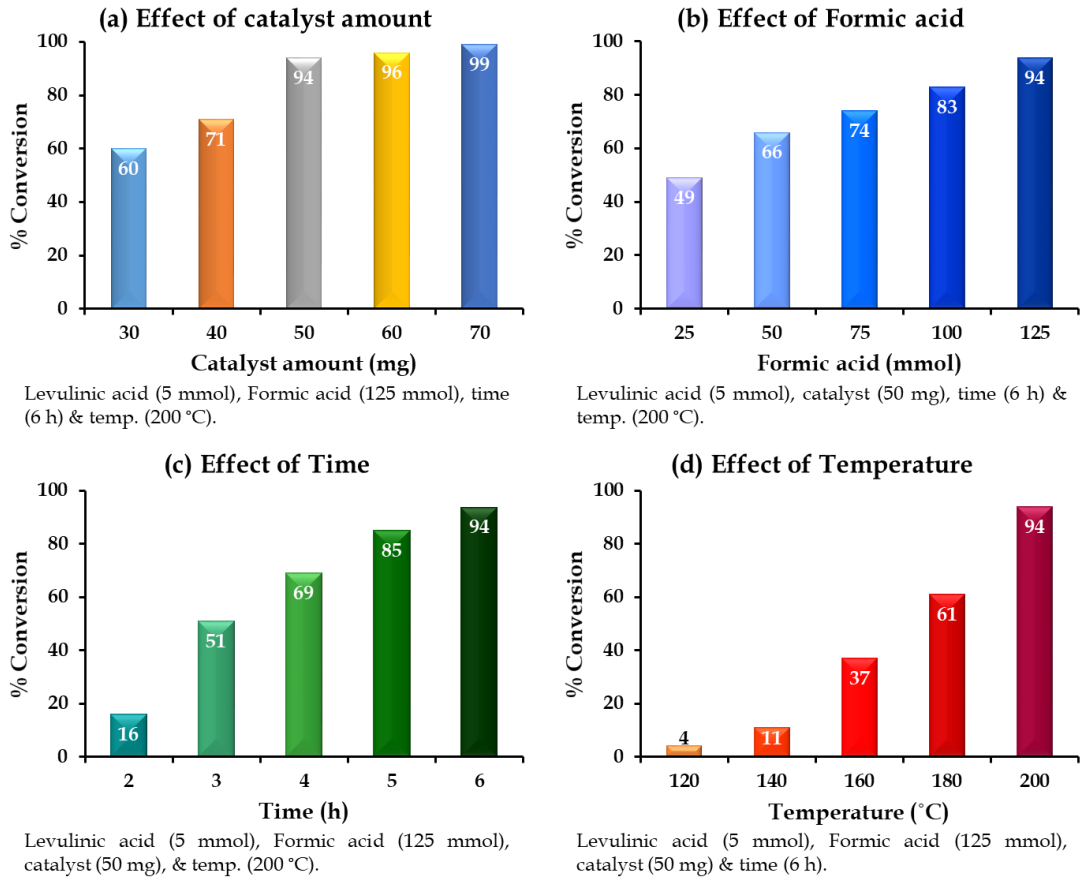

Figure 10. Optimization of reaction parameters

Based on the above studies, the optimized condition for 94% conversion are: catalyst amount (50 mg), levulinic acid (5 mmol), formic acid (125 mmol), temp. (200 ^{0}C), time (6 h), sub/cat (279/1), TON (204).

Control experiments for all the three reactions indicate that Ni is the real active species responsible for the reaction. Whereas leaching and recycling test confirms the no emission of NiNPs as well as PMo_{12} from the support up to three catalytic runs. Heterogeneity test also confirms the true heterogeneous nature of the catalyst during the reactions.

Elemental analysis of regenerated catalyst (figure 11a) shows the presence of all the expected elements andthe found values for Ni (0.28 wt%) and Mo (14.13 wt%) are in good agreement with the theoretical values (Ni, 0.82 wt % and W, 14.16 wt%). FT-IR (figure 11b) show the presence of all the characteristic bands of fresh catalyst (Ni-PMo_{12}/ZrO_2), which confirms the retention of the

Keggin structure. The XPS spectra (figure 11c) indicates the presence of Ni (0) as well as Mo in VI oxidation states, confirmed the in situ formation of NiNPs.

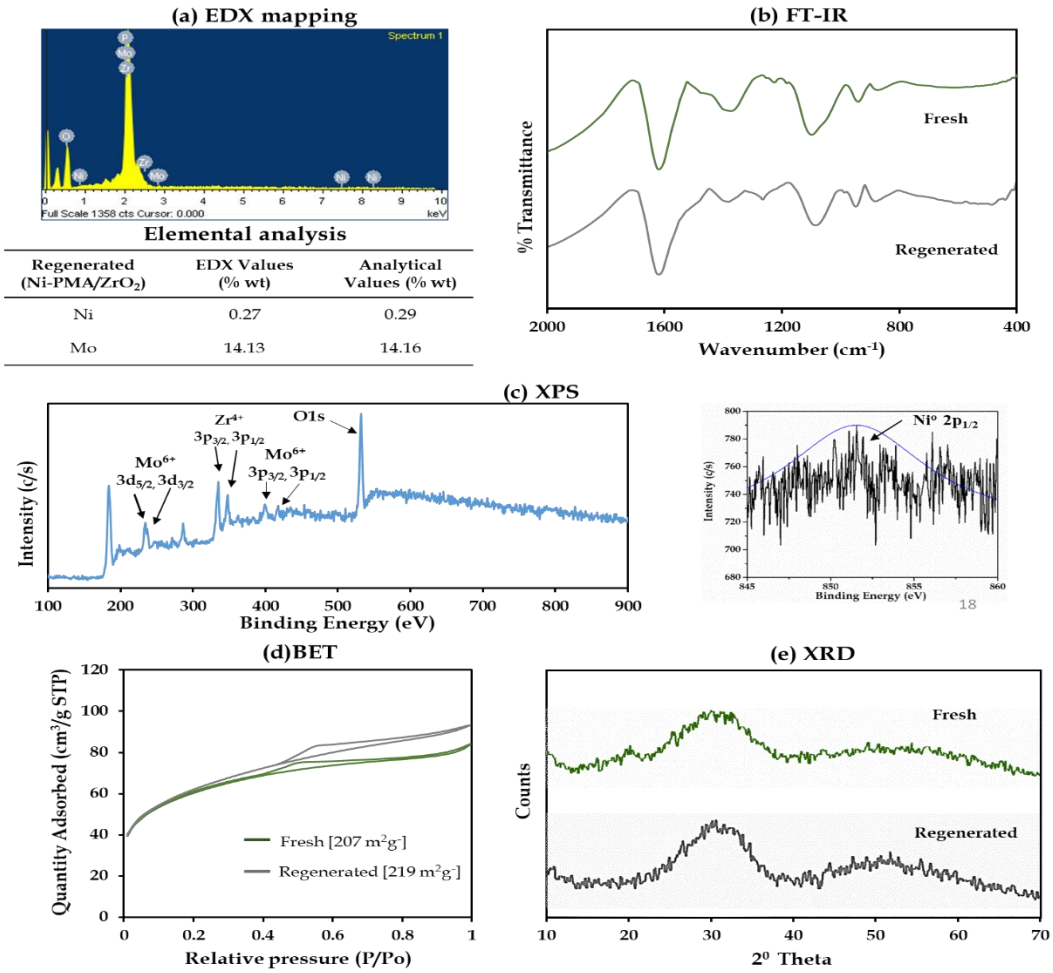

Figure 11. (a) EDX mapping & elemntal analysis, (b) FT-IR spectra, (c) XPS, (d) XPS, (d) BET and (e) XRD of regenerated catalyst

The BET surface area of R-Ni-PMo_{12}/ZrO_2 was found to be 219 m^2 g^{-1}, whereas drastic increase in surface indicates the formation of Ni NPs. The N_2 sorption isotherm (figure 11d) indicates the retention of the basic structure of the material even after loading. XRD pattern of regenerated catalyst (figure 11e) shows identical spectrum as fresh catalyst. The absence of any crystalline peaks confirms that there was no aggregates formed of NiNPS as well as retention of basic Keggin structure during the reaction. TEM and HRTEM images clearly shows the presence of NiNPs with homogeneous dispersion over the amorphous surface of the PMo_{12}/ZrO_2. HAADF- STEM show high dispersion Ni.

Chapter 2: Nickel salt of phosphomolybdic acid (NiHPMA): Synthesis, characterization and application for oxidative esterification

NiHPMA was synthesized by direct method as reported in the literature with modification. 1 g of PMA was dissolved in minimum amount of distilled water followed by the addition of a stoichiometric amount of aqueous $Ni(CH_3CO_2)_2$ (58.6 mg) solution dropwise. The resulting mixture was aged for 1 h at 80 °C and the excess water was evaporated to dryness on water bath. The resulting material was oven dried at 100 °C for 10 h, calcined at 300 °C for 2 h and the obtained green coloured material was designated as NiHPMA.

Elemental analysis show the presence of all the expected elements and the found values for EDX values of the elements (P:1.39%, Mo:57.15%, Ni:2.89%, O:38.57%) were in good agreement with the that of the calculated values(P:1.54%, Mo:57.34%, Ni:2.92%, O:38.20%). TGA shows initial weight loss of 2.46 % up to 100 ^{0}C, due to the removal of adsorbed water. Further, it shows 4.11 % weight loss up to 280 ^{0}C corresponding to removal of water of crystallization. Further, no appreciable weight loss was noticed, indicating the thermal stability of the synthesized material up to 500 ^{0}C. From the EDX and TGA, the chemical formula of the synthesized material was proposed as $NiH[PMo_{12}O_{40}].6H_2O$. The UV-visible spectrum of NiHPMA (figure 12a) shows the absorption peak at 230 nm due to the charge transfer between $O^{2-} \rightarrow Mo^{6+}$. Also it shows an absorption band at 396 nm, corresponding to the presence of Ni(II). FT-IR and Raman spectra (figure 12 b & c) of NiHPMA show the presence of all the characteristic bands of PMA, which indicates the retention of the Keggin structure. The XPS spectra confirm the presence of Ni (II) and Mo (VI) oxidation states confirming no reduction of Mo(VI) during the synthesis of the materials.

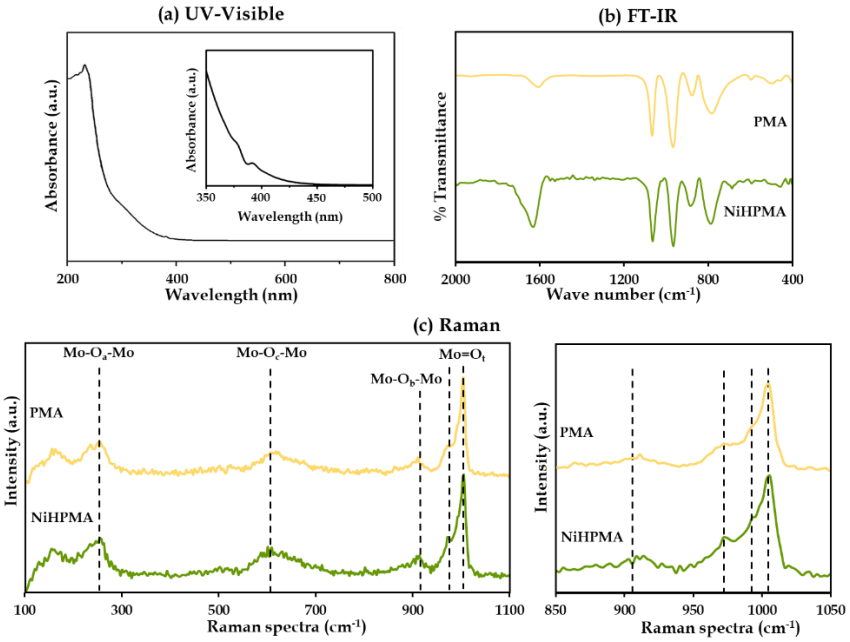

Figure 12. (a) UV-Visible, (b) FT-IR and (c) Raman spectra

Based on above studies, optimized conditions for maximum 68 % conversion with highest 86 % selectivity are: benzaldehyde, 10 mmol; H_2O_2, 30 mmol; catalyst, 5mg (active amount of Ni: 0.155 mg; catalyst/substrate ratio, 2.64×10^{-4}); methanol, 7 mL; temperature, 80 ^{0}C; and time, 6 hour, TON: 2576.

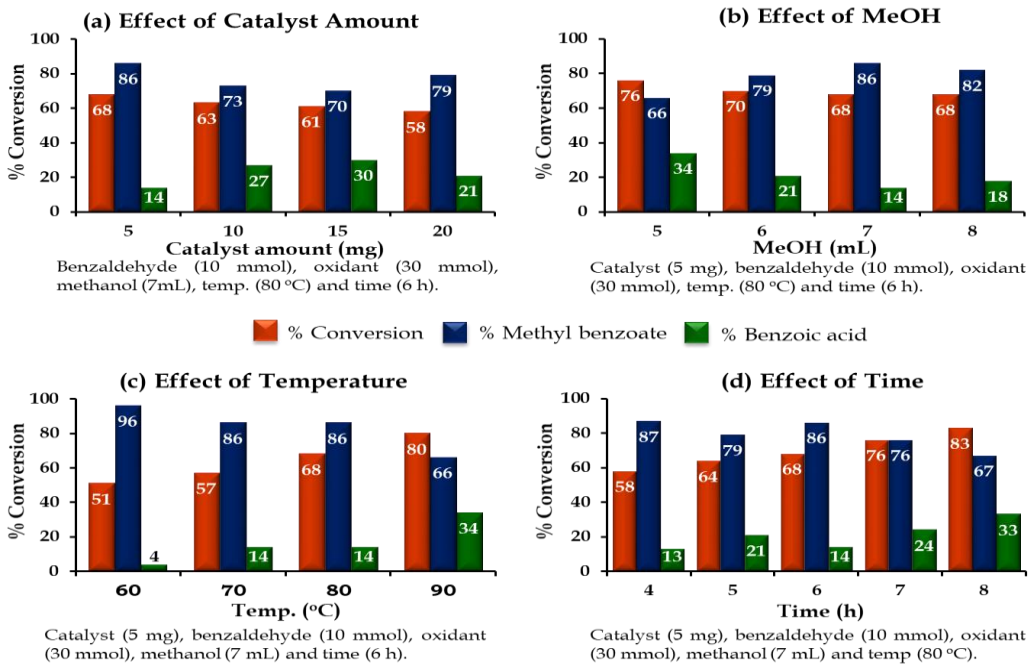

Figure 13. Optimization of reaction parameters

The catalyst is homogeneous even though it was easily recovered by simple heat to dryness method and used for number of cycles without significant change in conversion as well as selectivity.

Summary

Transition metal (Fe, Pd, and Ni) substituted or exchanged phosphomolybdic acid based heterogeneous catalysts were designed by insertion of metal in to the lacuna or exchange with available proton of phosphomolybdic acid. $PMo_{11}Fe$ and $PMo_{11}Pd$ synthesized by one pot method whereas Fe-PMo_{12}/ZrO_2, Pd-PMo_{12}/ZrO_2 and Ni-PMo_{12}/ZrO_2 were synthesized by exchanged method. NiHPMA synthesized by salt method. All the synthesized materials were characterized by elemental analysis, TGA, FT-IR, Raman spectara, UV-Visible, ^{31}P MAS NMR, ESR, XPS, powder XRD, BET, TEM, HRTEM and SAAD-HRTEM.

The efficiency of $PMo_{11}Fe$ and Fe-PMo_{12}/ZrO_2 were evaluated for alkene hydrogenation (Styrene and cyclohexene respectively). Whereas efficiency of Pd-PMo_{12}/ZrO_2 was evaluated for Suzuki–Miyaura cross coupling & One-pot Suzuki–Miyaura cross coupling/ nitro hydrogenation. The efficiency of $PMo_{11}Pd$ and Ni-PMo_{12}/ZrO_2 was evaluated for levulinic acid hydrogenation. To achieve maximum conversion and selectivity towards desired product various reaction parameters such as temperature, pressure, time, solvent and solvent ratio were optimized for all reaction.

For all the catalytic systems, the heterogeneity test and recycling tests were performed under optimized conditions, and the result showed the true heterogeneous nature of all the systems and can be used up to 3 catalytic runs and can be used for more. The regenerated catalysts were characterized by elemental analysis, FT-IR, XRD, ESR and XPS which confirmed the stability of the catalyst under optimized conditions.

References

1. A. Tézé, G. Hervé, Inorg. Synth. **1990**, 27, 85.
2. Dong-Xiao Wang, Ya-Guang Chen, Shan Wei, Xiao-Min Li, Inorganica Chimi. Acta **2014**, 415, 146–150.
3. Chemical Reviews, Polyoxometalates (Ed.: C. L. Hill), **1998**.
4. U. Kortz, Y. P. Jeannin, A. Teze, G. Herve, S. Isber, Inorg. Chem. **1999**, 38, 3670-3675.

5. Z. Luo, P. Kogerler, R. Cao, I. Hakim, C. L. Hill, Dalton Trans., **2008**, 54–58.
6. K. Kamata, S. Yamaguchi, M. Kotani, K. Yamaguchi, N. Mizuno, Angew. Chem. **2008**, 120, 2441 –2444.
7. N. Mizuno, Int. J. Soc. Mater. Eng. Resour. **2002**, 10, 135-136.
8. Y. Kikukawa, K. Suzuki, K. Yamaguchi, N. Mizuno, Inorg. Chem. **2013**, 52, 8644−8652.
9. S. Yamaguchi, Y. Kikukawa, K. Tsuchida, Y. Nakagawa, K. Uehara, K. Yamaguchi, N. Mizuno, Inorg. Chem. **2007**, 46, 8502-8504.
10. K. Patel, P. Shringarpure, A. Patel, *Transition Met. Chem.*, **2011**, 36, 171–177.
11. A. Patel, J. Patel, Catal. Lett. (2021). https://doi.org/10.1007/s10562-021-03838-8
12. A. Patel, J. Patel, Mol. Catal. 513 (2021) 111827.
13. P. Singh, S. Mishra, A. Sahoo, S. Patra, Sci. Rep. 11 (2021) 9305.
14. Y. Liu, X. Wu, Z. Li1, J. Zhang, S. Liu, S. Liu, L. Gu, L. R. Zheng, J Li , D. Wang, Y. Li, Nat. Commun. 12 (2021) 4205.

Jaykumar Patel
Research Scholar

Prof. (Dr.) Anjali Patel
Research Supervisor

Prof. Ashutosh Badekar
Offg. Head
Department of Chemistry